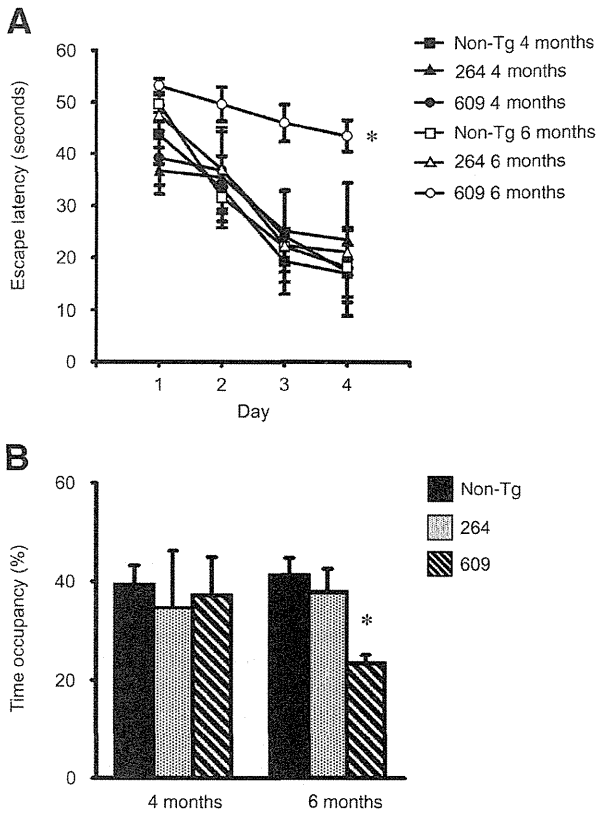

Figure 6 Memory impairment in tau Tg mice. The spatial reference memory of Tg mice was assessed by the Morris water maze at 4 and 6 months of age. **A:** Mice were trained to swim to a hidden platform for 4 consecutive days (five trials per day) (n = 9 at 4 months and n = 10 at 6 months for non-Tg littermates; n = 6 at 4 months and n = 10 at 6 months for lines 264 and 609). No difference in memory among non-Tg littermates, line 264, and line 609 was observed at 4 months of age. At 6 months of age, line 609 exhibited significantly longer latency than line 264 and non-Tg littermates. *P = 0.0011 versus 6-month-old non-Tg, P = 0.0027 versus 6-month-old line 264 mice. **B:** Retention of memory was assessed by a probe trial on day 5. Data are given as time occupancy in the target quadrant. †P = 0.0098 versus non-Tg, P = 0.0352 versus line 264. Data are given as means ± SEM.

mutant Tg mice were detected at 8 months of age (data not shown). These results suggest that synapse loss began to occur from areas closer to the pcl in mutant Tg mice.

Then we examined synaptic function in the hippocampal CA3 region in 6-month-old mutant Tg mice (line 609) by electrophysiologic testing compared with age-matched non-Tg littermates. At first, basal synaptic transmission was examined in four different areas (the pcl, sl1, sl2, and sr), the main projection sites of mossy fibers. As shown in Figure 5, A and B, significant lowering of I/O performance was observed in the pcl of mutant Tg mice. The same, but not significant, tendency was also detected in the sl1, and a somewhat inverse tendency was recorded in the more distal area of sl2, suggesting that basal synaptic transmission in mutant Tg mice was impaired in a manner depending on the distance from the pcl. This geometric feature of synaptic dysfunction seems to reflect the reduced synaptic density in this region (Figure 4). Next, long-term synaptic plasticity was examined by measuring LTP. In this experiment, we selected a recording point that showed good I/O performance from the sl1/2 area to minimize the influence of the differences in basal synaptic transmission. Again, significant impairment of LTP was observed in mutant Tg mice (Figure 5C). Thus, synapse loss and dysfunction in the hippocampus were shown to occur at the same time frame as the appearance of abnormally phosphorylated tau (Figure 2) in mutant Tg mice.

We also assessed the spatial reference memory of mice using the Morris water maze at 4 and 6 months of age. Mice were trained for 4 days to memorize the location of a hidden platform in a swimming pool, and the time required to reach the platform was measured as escape latency in each trial (Figure 6A). At 4 months of age, there were no differences in cognitive function among non-Tg littermates, line 264, and line 609. However, at 6 months of age, memory acquisition in line 609 got significantly worse, with longer escape latencies than those in non-Tg littermates. Probe trials with the platform removed at day 5 also revealed that memory retention in line 609 was significantly lower than that in non-Tg littermates at 6 months of age (Figure 6B). In contrast, line 264 exhibited no defects in memory acquisition and retention even at 6 months of age. No differences in locomotor activities were observed among the three groups.

Glial Activation in Intronic Mutant Mice

Because glial cell–mediated neuroinflammation is implicated in the pathogenesis of neurodegenerative diseases, we examined the occurrence of glial activation in Tg mice by IHC analysis. Brain sections at various ages were stained with antibodies to Iba-1 (Figure 7, A–H) and GFAP (Figure 7, I–P), which are markers for microglia and astrocytes, respectively. Non-Tg littermates exhibited no intense staining with these antibodies under the staining conditions even at 24 months (Figure 7, E and M). Line 264 possessed almost no GFAP-positive cells (Figure 7N) and only a few Iba-1–positive cells (Figure 7F) in the hippocampus at 24 months of age. In contrast, lines 609 and 784 began to display Iba-1–positive cells at 12 months of age (Figure 7, C and D) and GFAP-positive cells at 24 months of age (Figure 7, O and P) in the cerebral cortex and hippocampus. The apparently positive staining presumably reflects increased expression of these marker proteins, implying activation of the glial cells. Quantification of Iba-1–positive cells in the hippocampal CA1 region (Figure 7Q) and of GFAP-positive cells in the hippocampal CA2/3 region (Figure 7R) at 24 months of age indicates significantly increased activation of microglia and astrocytes in lines 609 and 784.

Neuronal Loss in Intronic Mutant Mice

Most tau Tg mice expressing missense mutations have been shown to display age-dependent neuronal loss. We questioned whether neuronal loss also occurs in intronic mutant

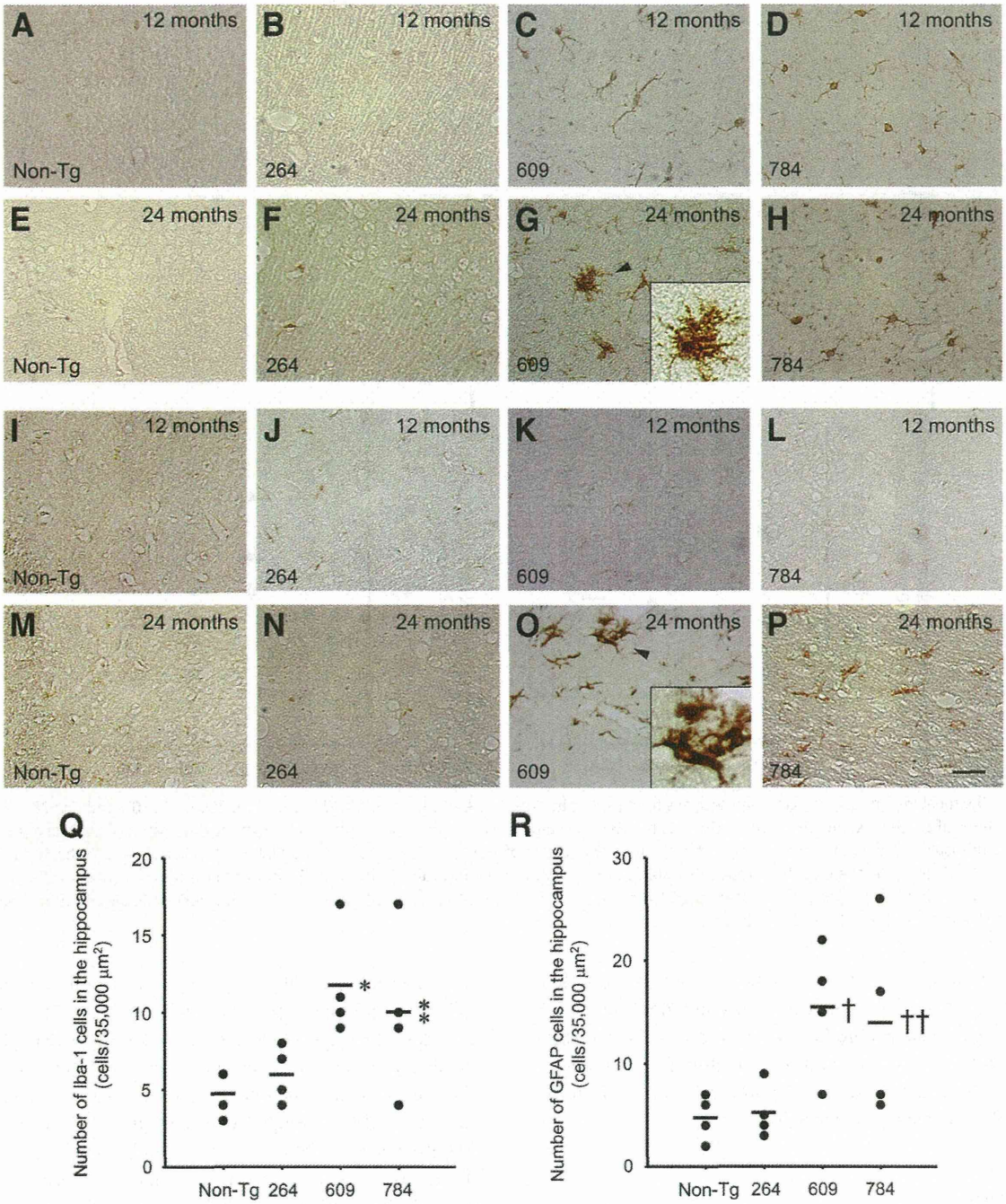

Figure 7 Glial activation in tau Tg mice. Brain sections from non-Tg littermates (**A, E, I,** and **M**), line 264 (**B, F, J,** and **N**), line 609 (**C, G, K,** and **O**), and line 784 (**D, H, L,** and **P**) at various ages were stained with antibodies to the microglia marker Iba-1 (**A**–**H**) and the astrocyte marker GFAP (**I**–**P**). Iba-1 images were taken from the hippocampal CA1 region at 12 and 24 months of age, and GFAP images were from the hippocampal CA2/3 region at the same ages. Lines 609 and 784 began to exhibit Iba-1–positive cells at 12 months of age (**C** and **D**), and GFAP-positive cells at 24 months of age (**O** and **P**). **Insets:** Extended images of Iba-1– or GFAP-positive cells indicated with **arrowheads**. Scale bar = 30 μm. **Q:** Iba-1–positive cells in the hippocampal CA1 region (220 × 160 μm) at 24 months of age were counted. $^{*}P = 0.0140$ versus non-Tg, $P = 0.0359$ versus line 264; $^{**}P = 0.0433$ versus non-Tg ($n = 4$). **R:** GFAP-positive cells in the hippocampal CA2/3 region (220 × 160 μm) at 24 months of age were counted. $^{\dagger}P = 0.0249$ versus non-Tg, $P = 0.0310$ versus line 264; $^{\dagger\dagger}P = 0.0477$ versus non-Tg ($n = 4$). The dots represent the measured values in each mouse and the horizontal lines show the mean values.

Tg mice. Brain sections at 18 and 24 months of age were stained with an antibody to NeuN, a marker of mature neurons (Figure 8A–H). Line 264 showed no significant difference from non-Tg littermates in the number of NeuN-positive cells at 24 months of age in the hippocampus and cerebral cortex (Figure 8, I and J). In contrast, lines 609 and 784 exhibited a significant decrease in mature neurons in the hippocampal CA1 region compared with non-Tg littermates at 24 months of age (Figure 8I). The same, but not significant, tendency was also observed in the retrosplenial region

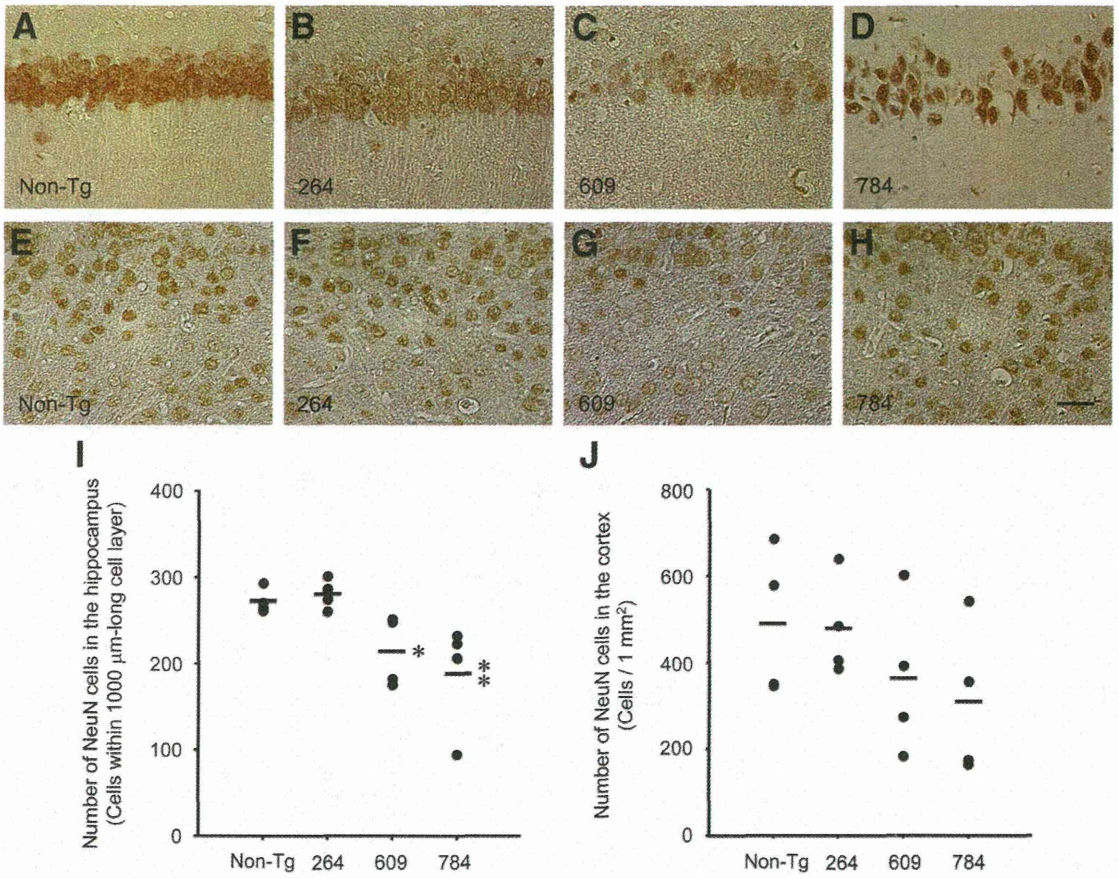

Figure 8 Neuronal loss in tau Tg mice. Brain sections from non-Tg littermates (**A** and **E**), line 264 (**B** and **F**), line 609 (**C** and **G**), and line 784 (**D** and **H**) at 18 and 24 months of age were stained with an antibody to the mature neuron marker NeuN. Images were taken from the CA1 region of the hippocampus (**A**–**D**) and from the retrosplenial region of the cerebral cortex (**E**–**H**) at 24 months of age. Scale bar = 30 μm. **I** and **J**: NeuN-positive cells in the hippocampal CA1 region (within 1000 μm along the pcl) (**I**) and the retrosplenial region of the cerebral cortex (1 × 1 mm) (**J**) at 24 months of age were counted. $^{*}P = 0.0464$ versus non-Tg, $P = 0.0264$ versus line 264; $^{**}P = 0.0023$ versus non-Tg, $P = 0.0013$ versus line 264 ($n = 4$). The dots represent the measured values in each mouse and the horizontal lines show the mean values.

of the cerebral cortex at 24 months of age (Figure 8J). Apparent neuronal loss, however, was not detected at 18 months of age. Taken together, these findings indicate that just an alteration of tau exon 10 splicing is sufficient to trigger the pathologic cascade to neuronal death even in the absence of a tau missense mutation.

Discussion

In the present study, we generated a new mouse model to understand FTDP-17. Mice were designed to mimic the isoform expression of tau in human brains with and without the intron 10 +16C→T mutation. The control and FTDP-17 model mice share the same tau minigene construct, including the intron 9, exon 10, and intron 10 sequences required for splicing machinery. As we intended, the introduced human tau trangenes and the endogenous mouse tau gene changed their isoform expression due to a development-dependent regulation *in vivo*. In control Tg mice, 3R tau was expressed at a juvenile age, whereas 3R and 4R human tau was expressed at an adult age, similar to in human brains.[11] In FTDP-17 Tg mice, which harbor the tau intron 10 +16C→T mutation, the expression pattern was similar except that 4R tau levels were higher than the control at adult age (Figure 1). The mutation examined herein has been shown to destabilize the predicted stem-loop structure of the 5′ splice site of exon 10 (splice donor site of intron 10) and, thereby, promote the binding of U1 small nuclear ribonucleic particles, a component of the spliceosome, which increases tau exon 10^{+} mRNA *in vitro*.[7,8,14,18] Herein, we found that this mutation, indeed, affected exon 10 splicing to increase 4R tau expression in adult mice and subsequently caused abnormal tau phosphorylation, synapse loss and dysfunction, memory impairment, glial activation, tangle formation, and neuronal loss in an age-dependent manner.

Synaptic and cognitive impairments in mutant Tg mice were associated with abnormal phosphorylation of tau in mossy fibers in the hippocampus at 6 months of age but not with that in neuronal cell bodies at 18 months of age. In contrast, neuronal loss occurred in the hippocampus at 24 month of age along with the appearance of tangles. These

results suggest that abnormal phosphorylation of tau in neurites contributes to synaptic and cognitive impairments, whereas somatic accumulation of aggregated tau leads to neurodegeneration. It is unclear, however, whether tangles are a marker for premature death or whether cells can survive the toxicity of tau aggregates by forming harmless tau inclusions. This latter theory is consistent with intracellular inclusions of insoluble tau aggregates not being toxic; rather, soluble tau oligomers are the cause of synaptic and cognitive dysfunction and neurodegeneration.[23–27] Toxic tau species in mutant Tg mice are to be the subject of future studies.

Note that the pathologic abnormalities we observed in these mice were induced just by changing the 3R/4R tau ratio, even in the absence of a missense mutation. Patients with this mutation have been reported to present prominent frontotemporal lobar atrophy with neuronal and glial tau inclusions in the form of neurofibrillary tangles and pre-tangles.[15,16,28–30] Biochemical analyses have revealed that sarkosyl-insoluble fractions from patient brains contain predominantly 4R tau, which assembles into twisted, ribbon-like filaments.[15,16] We show herein that mutant Tg mice reproduced neuropathologic abnormalities typical in patients: neuronal and glial tau inclusions, neuronal loss, 4R tau dominancy in sarkosyl-insoluble fractions, and tau filament formation.

There are many reports on FTDP-17 using mouse models,[12,13] and all describe tau missense mutations, such as G272V,[31] N279K,[17,32] V337M,[33] P301L,[34–39] P301S,[40,41] R406W,[42–44] the double mutations G272V/P301S[45] and K257T/P301S,[46] and the triple mutation G272V/P301L/R406W.[47] Most of these mutations have been shown to reduce the affinity of tau for microtubules[3,4] or to enhance the self-aggregation of tau.[5] Among them, only the N279K mutation, which is located in the 5′ region of exon 10, has been shown to affect exon 10 splicing in a way that increases 4R tau expression.[6] Dawson et al[32] generated Tg mice that express a human tau minigene, including introns with or without the N279K mutation and reported that this mutation caused an altered 3R/4R tau ratio from 1:1 at fetal age to almost 100% 4R tau at adult age. In addition, these mice exhibited age-dependent tau pathologic abnormalities at 18 weeks of age and motor and cognitive deficits at 23 weeks of age, suggesting that an imbalance of 3R and 4R tau expression could be a cause of tauopathy. However, it has remained unclear whether the pathologic abnormalities observed in those Tg mice were induced by the alteration in the tau isoform ratio or were the result of an aberrant property in the N279K mutant tau, as it was demonstrated that the presence of the N279K mutation exacerbates cognitive deficits in Tg mice expressing a single isoform of human tau.[17] The present intronic mutant Tg mice provide less ambiguous evidence that an imbalance of 3R and 4R tau expression leads to tau abnormalities even in the absence of mutant tau.

The present control Tg mice, which have the same regions of tau introns 9 and 10 as the present mutant Tg mice, showed a developmental change in exon 10 splicing similar to that in human brain and did not display any tau abnormalities. These findings seem to support our conclusion that the pathologic abnormalities observed in mutant Tg mice were due to the altered 3R/4R tau ratio. Nevertheless, we cannot exclude the possibility that the control Tg mice did not develop tau abnormalities because the expression levels of human tau in these mice were less than one-sixth those seen in mutant Tg mice. It has been shown, however, that an imbalance in 3R and 4R tau expression, rather than tau expression levels themselves, is critical for tau pathology in mice expressing wild-type human tau. Dawson et al[32] generated Tg mice that express 3R and 4R human tau at a ratio of 1:1 in the absence of the N279K mutation. The expression levels of human tau in these mice were more than two times endogenous mouse tau, but neither tau pathologic abnormalities nor motor and cognitive deficits were observed even at 52 weeks of age. Duff et al[48] generated Tg mice expressing all six isoforms of human tau by injecting human whole tau genes into mouse embryos. These mice expressed human tau levels that were more than three times endogenous mouse tau levels but did not exhibit tau abnormalities or motor deficits up to 8 months of age. In contrast, Tg mice expressing only 3R or 4R human tau did show tau pathology even at low levels of expression and, furthermore, motor deficits at high levels of expression.[49–54] For example, Götz et al[49] reported that their Tg mice ALZ7, which expressed the longest (4R) human tau isoform at levels equivalent to only 10% of endogenous mouse tau, displayed AT-8– and PHF-1–positive staining in neuronal cell bodies and processes at 3 months of age. Brion et al[50] generated Tg mice expressing the shortest (3R) human tau isoform at levels of approximately 20% endogenous mouse tau and observed abnormal tau phosphorylation in neuronal cell bodies and dendrites at 6 months of age. Although these mouse lines failed to produce neurofibrillary tangles and lacked obvious neurologic symptoms, they showed early tau pathologic abnormalities despite low levels of tau expression. Thus, unlike mouse tau, a balanced expression of 3R and 4R tau is presumably important for human tau to keep its normal condition at adult age.

In summary, we generated a new mouse model expressing wild-type human tau in the presence and absence of a tau intronic mutation linked to FTDP-17. Control Tg mice showed a normal developmental change of expression in tau isoform similar to human brains, whereas intronic mutant Tg mice selectively increased 4R-tau isoform and had pathologic abnormalities similar to patients with this mutation. The present Tg mice, therefore, could help elucidate the pathologic mechanism associated with tau proteins.

Acknowledgments

We thank Dr. Mark Mayford (Center for Neurobiology and Behavior, College of Physicians and Surgeons of Columbia University, and Howard Hughes Medical Institute) for

providing the pNN265 and pMM403 vectors and Rie Teraoka, Naomi Sakama, Reina Fujita, and Maiko Mori for technical assistance.

References

1. van Swieten J, Spillantini MG: Hereditary frontotemporal dementia caused by Tau gene mutations. Brain Pathol 2007, 17:63–73
2. Lee VM, Goedert M, Trojanowski JQ: Neurodegenerative tauopathies. Annu Rev Neurosci 2001, 24:1121–1159
3. Hasegawa M, Smith MJ, Goedert M: Tau proteins with FTDP-17 mutations have a reduced ability to promote microtubule assembly. FEBS Lett 1998, 437:207–210
4. Dayanandan R, Van Slegtenhorst M, Mack TG, Ko L, Yen SH, Leroy K, Brion JP, Anderton BH, Hutton M, Lovestone S: Mutations in tau reduce its microtubule binding properties in intact cells and affect its phosphorylation. FEBS Lett 1999, 446:228–232
5. Nacharaju P, Lewis J, Easson C, Yen S, Hackett J, Hutton M, Yen SH: Accelerated filament formation from tau protein with specific FTDP-17 missense mutations. FEBS Lett 1999, 447: 195–199
6. Hasegawa M, Smith MJ, Iijima M, Tabira T, Goedert M: FTDP-17 mutations N279K and S305N in tau produce increased splicing of exon 10. FEBS Lett 1999, 443:93–96
7. Grover A, Houlden H, Baker M, Adamson J, Lewis J, Prihar G, Pickering-Brown S, Duff K, Hutton M: 5′ splice site mutations in tau associated with the inherited dementia FTDP-17 affect a stem-loop structure that regulates alternative splicing of exon 10. J Biol Chem 1999, 274:15134–15143
8. Varani L, Hasegawa M, Spillantini MG, Smith MJ, Murrell JR, Ghetti B, Klug A, Goedert M, Varani G: Structure of tau exon 10 splicing regulatory element RNA and destabilization by mutations of frontotemporal dementia and parkinsonism linked to chromosome 17. Proc Natl Acad Sci U S A 1999, 96:8229–8234
9. Goedert M, Spillantini MG, Jakes R, Rutherford D, Crowther RA: Multiple isoforms of human microtubule-associated protein tau: sequences and localization in neurofibrillary tangles of Alzheimer's disease. Neuron 1989, 3:519–526
10. Kosik KS, Orecchio LD, Bakalis S, Neve RL: Developmentally regulated expression of specific tau sequences. Neuron 1989, 2: 1389–1397
11. Takuma H, Arawaka S, Mori H: Isoforms changes of tau protein during development in various species. Brain Res Dev Brain Res 2003, 142:121–127
12. Frank S, Clavaguera F, Tolnay M: Tauopathy models and human neuropathology: similarities and differences. Acta Neuropathol 2008, 115:39–53
13. Denk F, Wade-Martins R: Knock-out and transgenic mouse models of tauopathies. Neurobiol Aging 2009, 30:1–13
14. Hutton M, Lendon CL, Rizzu P, Baker M, Froelich S, Houlden H, et al: Association of missense and 5′-splice-site mutations in tau with the inherited dementia FTDP-17. Nature 1998, 393:702–705
15. Goedert M, Spillantini MG, Crowther RA, Chen SG, Parchi P, Tabaton M, Lanska DJ, Markesbery WR, Wilhelmsen KC, Dickson DW, Petersen RB, Gambetti P: Tau gene mutation in familial progressive subcortical gliosis. Nat Med 1999, 5:454–457
16. Pickering-Brown SM, Richardson AM, Snowden JS, McDonagh AM, Burns A, Braude W, Baker M, Liu WK, Yen SH, Hardy J, Hutton M, Davies Y, Allsop D, Craufurd D, Neary D, Mann DM: Inherited frontotemporal dementia in nine Br families associated with intronic mutations in the tau gene. Brain 2002, 125:732–751
17. Taniguchi T, Doe N, Matsuyama S, Kitamura Y, Mori H, Saito N, Tanaka C: Transgenic mice expressing mutant (N279K) human tau show mutation dependent cognitive deficits without neurofibrillary tangle formation. FEBS Lett 2005, 579:5704–5712
18. Yamashita T, Tomiyama T, Li Q, Numata H, Mori H: Regulation of tau exon 10 splicing by a double stem-loop structure in mouse intron 10. FEBS Lett 2005, 579:241–244
19. Mayford M, Bach ME, Huang YY, Wang L, Hawkins RD, Kandel ER: Control of memory formation through regulated expression of a CaMKII transgene. Science 1996, 274:1678–1683
20. Goedert M, Spillantini MG, Cairns NJ, Crowther RA: Tau proteins of Alzheimer paired helical filaments: abnormal phosphorylation of all six brain isoforms. Neuron 1992, 8:159–168
21. Tomiyama T, Matsuyama S, Iso H, Umeda T, Takuma H, Ohnishi K, Ishibashi K, Teraoka R, Sakama N, Yamashita T, Nishitsuji K, Ito K, Shimada H, Lambert MP, Klein WL, Mori H: A mouse model of amyloid β oligomers: their contribution to synaptic alteration, abnormal tau phosphorylation, glial activation, and neuronal loss in vivo. J Neurosci 2010, 30:4845–4856
22. Gallyas F: Silver staining of Alzheimer's neurofibrillary changes by means of physical development. Acta Morphol Acad Sci Hung 1971, 19:1–8
23. Santacruz K, Lewis J, Spires T, Paulson J, Kotilinek L, Ingelsson M, Guimaraes A, DeTure M, Ramsden M, McGowan E, Forster C, Yue M, Orne J, Janus C, Mariash A, Kuskowski M, Hyman B, Hutton M, Ashe KH: Tau suppression in a neurodegenerative mouse model improves memory function. Science 2005, 309:476–481
24. Berger Z, Roder H, Hanna A, Carlson A, Rangachari V, Yue M, Wszolek Z, Ashe K, Knight J, Dickson D, Andorfer C, Rosenberry TL, Lewis J, Hutton M, Janus C: Accumulation of pathological tau species and memory loss in a conditional model of tauopathy. J Neurosci 2007, 27:3650–3662
25. Patterson KR, Remmers C, Fu Y, Brooker S, Kanaan NM, Vana L, Ward S, Reyes JF, Philibert K, Glucksman MJ, Binder LI: Characterization of prefibrillar Tau oligomers in vitro and in Alzheimer disease. J Biol Chem 2011, 286:23063–23076
26. Fox LM, William CM, Adamowicz DH, Pitstick R, Carlson GA, Spires-Jones TL, Hyman BT: Soluble tau species, not neurofibrillary aggregates, disrupt neural system integration in a tau transgenic model. J Neuropathol Exp Neurol 2011, 70:588–595
27. Lasagna-Reeves CA, Castillo-Carranza DL, Sengupta U, Clos AL, Jackson GR, Kayed R: Tau oligomers impair memory and induce synaptic and mitochondrial dysfunction in wild-type mice. Mol Neurodegener 2011, 6:39
28. Janssen JC, Warrington EK, Morris HR, Lantos P, Brown J, Revesz T, Wood N, Khan MN, Cipolotti L, Fox NC, Rossor MN: Clinical features of frontotemporal dementia due to the intronic tau 10(+16) mutation. Neurology 2002, 58:1161–1168
29. Lantos PL, Cairns NJ, Khan MN, King A, Revesz T, Janssen JC, Morris H, Rossor MN: Neuropathologic variation in frontotemporal dementia due to the intronic tau 10(+16) mutation. Neurology 2002, 58:1169–1175
30. Doran M, du Plessis DG, Ghadiali EJ, Mann DM, Pickering-Brown S, Larner AJ: Familial early-onset dementia with tau intron 10 + 16 mutation with clinical features similar to those of Alzheimer disease. Arch Neurol 2007, 64:1535–1539
31. Götz J, Tolnay M, Barmettler R, Chen F, Probst A, Nitsch RM: Oligodendroglial tau filament formation in transgenic mice expressing G272V tau. Eur J Neurosci 2001, 13:2131–2140
32. Dawson HN, Cantillana V, Chen L, Vitek MP: The tau N279K exon 10 splicing mutation recapitulates frontotemporal dementia and parkinsonism linked to chromosome 17 tauopathy in a mouse model. J Neurosci 2007, 27:9155–9168
33. Tanemura K, Akagi T, Murayama M, Kikuchi N, Murayama O, Hashikawa T, Yoshiike Y, Park JM, Matsuda K, Nakao S, Sun X, Sato S, Yamaguchi H, Takashima A: Formation of filamentous tau aggregations in transgenic mice expressing V337M human tau. Neurobiol Dis 2001, 8:1036–1045
34. Lewis J, McGowan E, Rockwood J, Melrose H, Nacharaju P, Van Slegtenhorst M, Gwinn-Hardy K, Paul Murphy M, Baker M, Yu X, Duff K, Hardy J, Corral A, Lin WL, Yen SH, Dickson DW, Davies P,

Hutton M: Neurofibrillary tangles, amyotrophy and progressive motor disturbance in mice expressing mutant (P301L) tau protein. Nat Genet 2000, 25:402–405
35. Götz J, Chen F, Barmettler R, Nitsch RM: Tau filament formation in transgenic mice expressing P301L tau. J Biol Chem 2001, 276:529–534
36. Higuchi M, Zhang B, Forman MS, Yoshiyama Y, Trojanowski JQ, Lee VM: Axonal degeneration induced by targeted expression of mutant human tau in oligodendrocytes of transgenic mice that model glial tauopathies. J Neurosci 2005, 25:9434–9443
37. Ramsden M, Kotilinek L, Forster C, Paulson J, McGowan E, SantaCruz K, Guimaraes A, Yue M, Lewis J, Carlson G, Hutton M, Ashe KH: Age-dependent neurofibrillary tangle formation, neuron loss, and memory impairment in a mouse model of human tauopathy (P301L). J Neurosci 2005, 25:10637–10647
38. Terwel D, Lasrado R, Snauwaert J, Vandeweert E, Van Haesendonck C, Borghgraef P, Van Leuven F: Changed conformation of mutant Tau-P301L underlies the moribund tauopathy, absent in progressive, nonlethal axonopathy of Tau-4R/2N transgenic mice. J Biol Chem 2005, 280:3963–3973
39. Murakami T, Paitel E, Kawarabayashi T, Ikeda M, Chishti MA, Janus C, Matsubara E, Sasaki A, Kawarai T, Phinney AL, Harigaya Y, Horne P, Egashira N, Mishima K, Hanna A, Yang J, Iwasaki K, Takahashi M, Fujiwara M, Ishiguro K, Bergeron C, Carlson GA, Abe K, Westaway D, St George-Hyslop P, Shoji M: Cortical neuronal and glial pathology in TgTauP301L transgenic mice: neuronal degeneration, memory disturbance, and phenotypic variation. Am J Pathol 2006, 169:1365–1375
40. Allen B, Ingram E, Takao M, Smith MJ, Jakes R, Virdee K, Yoshida H, Holzer M, Craxton M, Emson PC, Atzori C, Migheli A, Crowther RA, Ghetti B, Spillantini MG, Goedert M: Abundant tau filaments and nonapoptotic neurodegeneration in transgenic mice expressing human P301S tau protein. J Neurosci 2002, 22: 9340–9351
41. Yoshiyama Y, Higuchi M, Zhang B, Huang SM, Iwata N, Saido TC, Maeda J, Suhara T, Trojanowski JQ, Lee VM: Synapse loss and microglial activation precede tangles in a P301S tauopathy mouse model. Neuron 2007, 53:337–351
42. Tatebayashi Y, Miyasaka T, Chui DH, Akagi T, Mishima K, Iwasaki K, Fujiwara M, Tanemura K, Murayama M, Ishiguro K, Planel E, Sato S, Hashikawa T, Takashima A: Tau filament formation and associative memory deficit in aged mice expressing mutant (R406W) human tau. Proc Natl Acad Sci U S A 2002, 99:13896–13901
43. Zhang B, Higuchi M, Yoshiyama Y, Ishihara T, Forman MS, Martinez D, Joyce S, Trojanowski JQ, Lee VM: Retarded axonal transport of R406W mutant tau in transgenic mice with a neurodegenerative tauopathy. J Neurosci 2004, 24:4657–4667
44. Ikeda M, Shoji M, Kawarai T, Kawarabayashi T, Matsubara E, Murakami T, Sasaki A, Tomidokoro Y, Ikarashi Y, Kuribara H, Ishiguro K, Hasegawa M, Yen SH, Chishti MA, Harigaya Y, Abe K, Okamoto K, St George-Hyslop P, Westaway D: Accumulation of filamentous tau in the cerebral cortex of human tau R406W transgenic mice. Am J Pathol 2005, 166:521–531
45. Schindowski K, Bretteville A, Leroy K, Bégard S, Brion JP, Hamdane M, Buée L: Alzheimer's disease-like tau neuropathology leads to memory deficits and loss of functional synapses in a novel mutated tau transgenic mouse without any motor deficits. Am J Pathol 2006, 169:599–616
46. Rosenmann H, Grigoriadis N, Eldar-Levy H, Avital A, Rozenstein L, Touloumi O, Behar L, Ben-Hur T, Avraham Y, Berry E, Segal M, Ginzburg I, Abramsky O: A novel transgenic mouse expressing double mutant tau driven by its natural promoter exhibits tauopathy characteristics. Exp Neurol 2008, 212:71–84
47. Lim F, Hernández F, Lucas JJ, Gómez-Ramos P, Morán MA, Avila J: FTDP-17 mutations in tau transgenic mice provoke lysosomal abnormalities and Tau filaments in forebrain. Mol Cell Neurosci 2001, 18:702–714
48. Duff K, Knight H, Refolo LM, Sanders S, Yu X, Picciano M, Malester B, Hutton M, Adamson J, Goedert M, Burki K, Davies P: Characterization of pathology in transgenic mice over-expressing human genomic and cDNA tau transgenes. Neurobiol Dis 2000, 7: 87–98
49. Götz J, Probst A, Spillantini MG, Schäfer T, Jakes R, Bürki K, Goedert M: Somatodendritic localization and hyperphosphorylation of tau protein in transgenic mice expressing the longest human brain tau isoform. EMBO J 1995, 14:1304–1313
50. Brion JP, Tremp G, Octave JN: Transgenic expression of the shortest human tau affects its compartmentalization and its phosphorylation as in the pretangle stage of Alzheimer's disease. Am J Pathol 1999, 154: 255–270
51. Ishihara T, Hong M, Zhang B, Nakagawa Y, Lee MK, Trojanowski JQ, Lee VM: Age-dependent emergence and progression of a tauopathy in transgenic mice overexpressing the shortest human tau isoform. Neuron 1999, 24:751–762
52. Spittaels K, Van den Haute C, Van Dorpe J, Bruynseels K, Vandezande K, Laenen I, Geerts H, Mercken M, Sciot R, Van Lommel A, Loos R, Van Leuven F: Prominent axonopathy in the brain and spinal cord of transgenic mice overexpressing four-repeat human tau protein. Am J Pathol 1999, 155:2153–2165
53. Probst A, Götz J, Wiederhold KH, Tolnay M, Mistl C, Jaton AL, Hong M, Ishihara T, Lee VM, Trojanowski JQ, Jakes R, Crowther RA, Spillantini MG, Bürki K, Goedert M: Axonopathy and amyotrophy in mice transgenic for human four-repeat tau protein. Acta Neuropathol 2000, 99:469–481
54. Higuchi M, Ishihara T, Zhang B, Hong M, Andreadis A, Trojanowski J, Lee VM: Transgenic mouse model of tauopathies with glial pathology and nervous system degeneration. Neuron 2002, 35:433–446

Journal of Neuroscience Research

Journal of Neuroscience Research 91:1541–1550 (2013)

The E693Δ (Osaka) Mutation in Amyloid Precursor Protein Potentiates Cholesterol-Mediated Intracellular Amyloid β Toxicity Via Its Impaired Cholesterol Efflux

Sachiko Nomura,[1,2] Tomohiro Umeda,[1,2] Takami Tomiyama,[1,2]* and Hiroshi Mori[1,2]

[1]Department of Neuroscience, Osaka City University Graduate School of Medicine, Osaka, Japan
[2]Core Research for Evolutional Science and Technology, Japan Science and Technology Agency, Tokyo, Japan

It has been shown that amyloid β (Aβ) secretion regulates cholesterol efflux from cells and that the E693Δ (Osaka) mutation in amyloid precursor protein (APP) promotes intracellular accumulation of Aβ and thus reduces its secretion. These findings led us to speculate that APP with the Osaka mutation (APP_{OSK}) might have a defect in cholesterol efflux and thus cause cellular malfunction. We therefore examined the effects of this mutation on intracellular cholesterol transport and efflux in cultured cells. Upon cholesterol loading, APP_{OSK}-expressing cells exhibited higher levels of cellular cholesterol than wild-type APP-expressing cells, suggesting impaired cholesterol efflux. It is known that, after its internalization, cholesterol is transported from the endosomes to the endoplasmic reticulum (ER) and Golgi apparatus and then to the plasma membrane. In APP_{OSK}-expressing cells, cholesterol accumulated with Aβ in the ER and Golgi apparatus and alone in endosomes/lysosomes. These results imply that the mutation-induced disturbance of Aβ trafficking from the ER to the plasma membrane affects cholesterol transport to cause cholesterol accumulation in the ER and Golgi apparatus and, consequently, in endosomes. Furthermore, we detected an enhanced mitochondrial accumulation of Aβ and cholesterol in APP_{OSK}-expressing cells, and this was accompanied by an increase in the generation of reactive oxygen species (ROS). The present findings suggest that Aβ trafficking is important for intracellular cholesterol transport and efflux and that the Osaka mutation potentiates cholesterol-dependent exacerbation of intracellular Aβ toxicity, i.e. Aβ-induced ROS generation, by disturbing Aβ-mediated cholesterol efflux from the cell.

Key words: Alzheimer's disease; amyloid β (Aβ); cholesterol; mitochondria; reactive oxygen species (ROS)

Cerebral accumulation of amyloid β (Aβ) is a hallmark of Alzheimer's disease (AD). The E693Δ (Osaka) mutation in amyloid precursor protein (APP) has been shown to cause AD by enhanced formation of synaptotoxic Aβ oligomers (Tomiyama et al., 2008). This mutation is also characterized by a marked decrease in Aβ secretion (Tomiyama et al., 2008) and an increased Aβ accumulation within cells, probably resulting from disturbed Aβ trafficking from the endoplasmic reticulum (ER) to the plasma membrane (Nishitsuji et al., 2009). Transgenic (Tg) mice expressing APP with the Osaka mutation (APP_{OSK}) were found to display an intraneuronal accumulation of Aβ oligomers and subsequent synapse loss and memory impairment from 8 months and eventual neuronal loss at 24 months of age (Tomiyama et al., 2010). In cultured cells transfected with APP_{OSK} and brains of APP_{OSK}-Tg mice, Aβ oligomers accumulated in the ER, Golgi apparatus, ensosomes/lysosomes, autophagosomes, and mitochondria and caused ER stress, endosomal/lysosomal leakage, and mitochondrial dysfunction that led to apoptosis (Nishitsuji et al., 2009; Umeda et al., 2011).

High levels of plasma cholesterol are known to be a risk factor for AD (Solomon and Kivipelto, 2009; Stefani and Liguri, 2009). This is presumably because cholesterol affects APP processing to increase Aβ generation via

Contract grant sponsor: Ministry of Education, Culture, Sports, Science and Technology of Japan; Contract grant numbers: 21390271; 21500352; 23110514; Contract grant sponsor: Ministry of Health, Labour, and Welfare, Japan; Contract grant sponsor: Alzheimer's Association; Contract grant number: IIRG-09-132098.

*Correspondence to: Takami Tomiyama, PhD, Department of Neuroscience, Osaka City University Graduate School of Medicine, 1-4-3 Asahimachi, Abeno-ku, Osaka 545–8585, Japan. E-mail: tomi@med.osaka-cu.ac.jp

Received 22 November 2012; Revised 21 June 2013; Accepted 21 June 2013

Published online 16 September 2013 in Wiley Online Library (wileyonlinelibrary.com). DOI: 10.1002/jnr.23278

activation of both β- and γ-secretases (Frears et al., 1999; Xiong et al., 2008) and inhibition of α-secretase (Bodovitz and Klein, 1996). However, it remains unclear why high levels of cholesterol increase Aβ generation. After its internalization, cholesterol is transported from the endosomes to other compartments such as the ER and Golgi apparatus via the endosomal cholesterol transporters Niemann-Pick type C1 (NPC1) and NPC2 and cytosolic cholesterol transporters such as oxysterol-binding protein-related proteins (Chang et al., 2006; Prinz, 2007; Subramanian and Balch, 2008). Cholesterol is then transported from the ER and Golgi apparatus to the plasma membrane and excreted from the cell as a lipoprotein via membrane cholesterol transporters such as ATP-binding cassette transporter A1 (ABCA1) and extracellular apolipoproteins such as apoA and apoE (Chang et al., 2006; Yokoyama, 2006; Prinz, 2007). We have previously shown that, during its secretion, Aβ forms high-density lipoprotein (HDL)-like complexes with cellular cholesterol via ABCA1, leading to cholesterol efflux from cells (Umeda et al., 2010). Inhibition of Aβ production with β- and γ-secretase inhibitors resulted in increased levels of cellular cholesterol along with decreased secretion of cholesterol particles, whereas enhancement of Aβ production with an α-secretase inhibitor or by introducing the Swedish-type mutation into APP caused a marked reduction in cellular cholesterol levels (Umeda et al., 2010). These findings suggest a novel, apolipoprotein-like function of Aβ and may account for the biological significance of cholesterol-promoted Aβ generation.

This conclusion implies that certain APP mutations that decrease Aβ secretion may also disturb Aβ-mediated cholesterol efflux and induce cholesterol accumulation within a cell. Thus, we speculate that APP_{OSK} might have a defect in cholesterol efflux resulting from disturbed Aβ secretion and that this may cause cellular malfunction. For example, it has been shown that mitochondrial accumulation of cholesterol increases the susceptibility of neurons to $Aβ_{42}$-induced reactive oxygen species (ROS) generation, probably by the cholesterol-mediated depletion of mitochondrial glutathione, a critical antioxidant defense (Fernandez et al., 2009). In the present study, we therefore examined the effects of the Osaka mutation on intracellular cholesterol transport and efflux as well as ROS generation in cultured cells. Our findings suggest that Aβ trafficking is important for intracellular cholesterol transport and efflux and that the Osaka mutation potentiates cholesterol-mediated exacerbation of intracellular Aβ toxicity via its impaired cholesterol efflux.

MATERIALS AND METHODS

Chemicals and Antibodies

The cholesterol/methyl-β-cyclodextrin (MβCD) complex and the filipin complex were purchased from Sigma-Aldrich (St. Louis, MO). A rabbit polyclonal antibody to the C-terminal region of APP (C40) was prepared in our laboratories (Suga et al., 2004). A mouse monoclonal antibody to the N-terminus of Aβ (82E1; IBL, Takasaki, Japan) and rabbit polyclonal antibodies to actin (Sigma), the ER marker calnexin (Stressgen Bioreagents Corp., Ann Arbor, MI), and the Golgi marker RCAS1 (Cell Signaling Technology, Danvers, MA) were also purchased. LysoTracker Red (DND-99), MitoTracker Red (CMXRos), the ROS indicator 6-carboxy-2′,7′-dichlorodihydrofluorescein diacetate (carboxy H_2DCFDA), and Hoechst33342 were purchased from Molecular Probes (Eugene, OR). Alexa 488-conjugated anti-mouse IgG and Alexa 594-conjugated anti-rabbit IgG antibodies were also obtained from Molecular Probes, and cyanine 5 (Cy5)-conjugated rabbit IgG antibody was obtained from Jackson Immunoresearch (West Grove, PA).

APP Constructs

Wild-type and Osaka-mutant human APP_{695} cDNA constructs were prepared with the pCI mammalian expression vector (Promega, Madison, WI), as described previously (Nishitsuji et al., 2009).

Cellular Cholesterol

The human kidney line HEK293 cells were transfected with the APP constructs or an empty vector using Lipofectamine 2000 reagent (Invitrogen, Carlsbad, CA), and mouse neuroblastoma Neuro-2a cells and human astrocytoma U-251 MG (formerly known as U-373 MG) cells were transfected using Lipofectamine LTX reagent (Invitrogen). Two days after transfection, the cells were loaded with cholesterol by incubation at 4°C for 30 min with 1 mM cholesterol/MβCD complex in serum-free DMEM. The cholesterol loading media were replaced with fresh serum-free DMEM, and the cells were further incubated at 37°C for 6 hr (HEK293 and U-251 MG) or 1 hr (Neuro-2a). After being washed with PBS, the cells were harvested. Cellular cholesterol was extracted from the cell pellets and subjected to cholesterol assay using a Cholesterol/Cholesteryl Ester Quantitation Kit (BioVision, Mountain View, CA), as described previously (Umeda et al., 2010). The levels of APP expression were determined by Western blot with C40 antibody, as described previously (Umeda et al., 2010).

Aβ ELISA

HEK293, Neuro-2a, and U-251 MG cells were transfected with the APP constructs, loaded with cholesterol, and incubated for 6 hr or 1 hr after medium change, as described above. The culture media and cells were harvested for Aβ measurement. To extract intracellular Aβ, the cells were sonicated in 70% formic acid (FA) and centrifuged at 100,000*g* for 1 hr at room temperature. The supernatants were diluted tenfold in 1 M Tris solution (pH 11). Aβ concentrations in the culture media and neutralized FA extracts were determined using human Aβ ELISA kits (Wako Chemicals, Osaka, Japan). For the measurement of mutant Aβ, synthetic E22Δ-mutant $Aβ_{40}$ and $Aβ_{42}$ peptides were used to make standard curves.

Immunocytochemistry

Monkey kidney line COS-7 cells grown on coverslips coated with poly-L-lysine were transfected with the APP

constructs, loaded with cholesterol, and incubated for 6 hr after medium change, as described above. For imaging of the endosomes/lysosomes and mitochondria, cells were incubated with 75 nM LysoTracker Red or 200 nM MitoTracker Red in serum-free DMEM at 37°C for the last 45 min of the 6-hr incubation. The cells were fixed with 4% paraformaldehyde in PBS at room temperature for 30 min and permeabilized by immersion in PBS containing 0.2% Triton X-100 for 5 min. After blocking with 10% goat serum in PBS at room temperature for 1 hr, the cells were double stained with primary antibodies at room temperature for 1 hr, followed by Alexa 488-conjugated anti-mouse IgG and Alexa 594- or Cy5-conjugated anti-rabbit IgG antibody at room temperature for 20 min. For the imaging of cholesterol, the immunolabeled cells were stained with 125 μg/ml filipin in PBS for 15 min at room temperature before mounting. The stained specimens were mounted with Vectashield mounting medium (Vector, Burlingame, CA) and viewed under a Leica TCS SP5 confocal laser microscope (Leica, Wetzlar, Germany). Quantification of filipin and 82E1 (Aβ) intensity was performed in NIH ImageJ software.

ROS Generation

COS-7 cells were seeded into black 96-well microplates at a density of 1.3×10^4 cells/100 μl/well. The cells were transfected with APP constructs and loaded with cholesterol, as described above. After 5 hr of cholesterol loading, the plates were washed with Hanks' balanced salt solution (HBSS), and 20 μM carboxy H_2DCFDA in HBSS was added to each well. The plates were incubated at 37°C for 1 hr and washed with prewarmed HBSS. ROS-induced DCF fluorescence was measured using an excitation of 490 nm and emission of 535 nm in a multiplate reader (Wallac ARVO SX; Perkin Elmer, Wellesley, MA).

For the visualization of intracellular ROS, COS-7 cells were seeded onto glass coverslip-based dishes with grids (AGC Techno Glass Corp., Tokyo, Japan). The cells were transfected with APP constructs, loaded with cholesterol, and stained with carboxy H_2DCFDA, followed by counterstaining with Hoechst 33342. DCF fluorescence and phase-contrast images of cells were taken using a fluorescence microscope (Biozero BZ-8000; Keyence, Osaka, Japan) before cell fixation. The cells were then fixed and stained with C40 antibody, and images of the same fields on the coverslips were taken again with the same microscope.

Statistical Analysis

All values are expressed as mean ± SEM. Comparisons of means between two groups were performed using the unpaired Student's *t*-test, whereas those among multiple groups were performed using Tukey's post hoc test following one-way factorial ANOVA.

RESULTS

Aβ Secretion and Cellular Cholesterol Levels in APP_{OSK}-Transfected Cells

We initially examined the effect of the Osaka mutation on Aβ secretion and cellular cholesterol levels. Human kidney-derived HEK293 cells were transfected with wild-type APP (APP_{WT}), APP_{OSK}, and an empty vector (mock). There was no significant difference in APP expression levels between APP_{WT}- and APP_{OSK}-transfected cells (Fig. 1A). The cells were loaded with cholesterol by incubation with the cholesterol/MβCD complex for 30 min. This treatment increased cellular cholesterol levels to twice those in nontreated cells (Fig. 1A). The cholesterol loading media were replaced with fresh media lacking cholesterol, and the cells were further incubated for 6 hr. Compared with mock-transfected cells, APP_{WT}-transfected cells exhibited significantly lower levels of cholesterol, whereas APP_{OSK}-transfected cells showed similar levels (Fig. 1A). The Aβ concentrations in culture media of APP_{OSK}-transfected cells were significantly lower than those of APP_{WT}-transfected cells (Fig. 1B). Conversely, the levels of intracellular Aβ extracted from APP_{OSK}-transfected cells were significantly higher than those from APP_{WT}-transfected cells (Fig. 1C). Intracellular accumulation was more prominent with $Aβ_{42}$ than $Aβ_{40}$. These results indicate that cells with the Osaka mutation have a defect in cholesterol efflux because of disturbed Aβ secretion, as expected.

Similar experiments were performed using mouse neuroblastoma Neuro-2a cells. The cells transfected with APP_{WT}, APP_{OSK}, and an empty vector were loaded with cholesterol for 30 min and incubated for 1 hr after medium replacement. Again, APP_{WT}-transfected cells exhibited significantly lower levels of cellular cholesterol than mock-transfected cells, whereas APP_{OSK}-transfected cells showed similar levels (Fig. 2A). Also, the Aβ concentrations in culture media of APP_{OSK}-transfected cells were significantly lower than those of APP_{WT}-transfected cells (Fig. 2B). Thus, the inverse effects of the Osaka mutation on Aβ secretion and cellular cholesterol levels were confirmed in neuronal cells.

Astrocytes are known to secrete lipoproteins constitutively to deliver cholesterols to neurons. Thus we examined Aβ secretion and cellular cholesterol levels using human astrocytoma U-251 MG cells. We detected, however, neither Aβ secretion from this cell line even after APP transfection nor significant differences in cellular cholesterol levels among APP_{WT}-, APP_{OSK}-, and mock-transfected cells (data not shown). Astrocytes have been shown to express very low levels of the β-secretase enzyme BACE1 in their resting state (Zhao et al., 1996; Rossner et al., 2001), so these results suggest that cholesterol efflux from astrocytes occurs independently of Aβ secretion at least under normal conditions.

Intracellular Accumulation of Aβ and Cholesterol in APP_{OSK}-Expressing Cells

To visualize the intracellular accumulation of cholesterol and Aβ in APP_{OSK}-expressing cells, we stained cells with filipin, a fluorescent dye capable of binding to cholesterol, in combination with antibodies to APP (C40, rabbit) and Aβ (82E1, mouse). We used monkey kidney-derived COS-7 cells in this experiment, because their cell

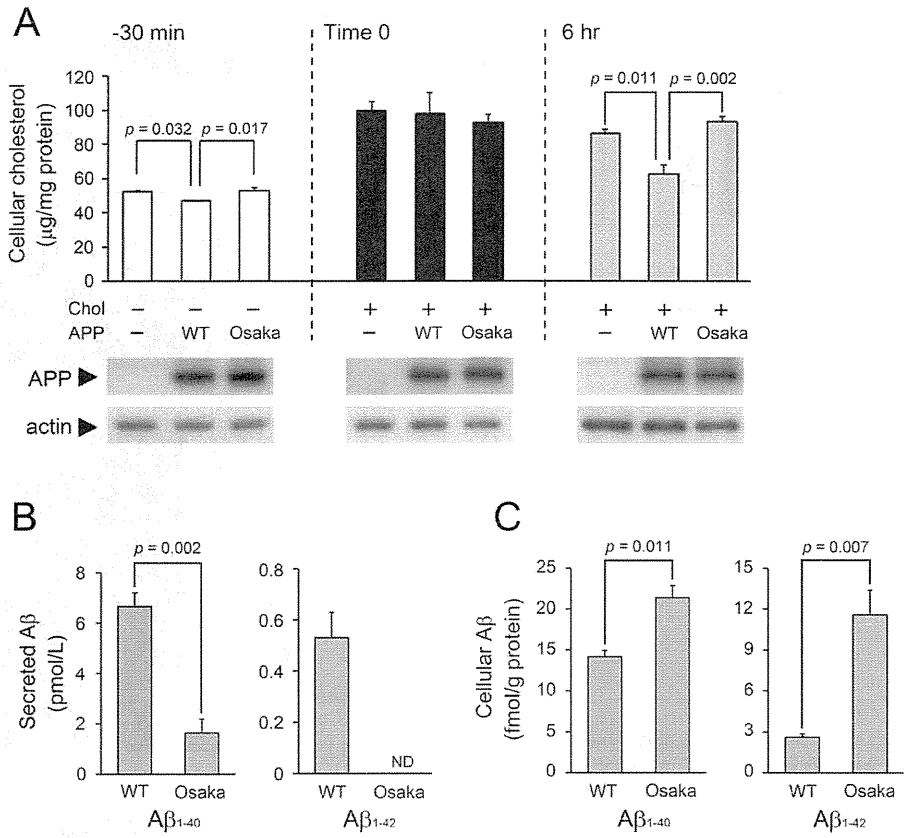

Fig. 1. Impaired Aβ secretion and sustained cellular cholesterol levels in APP_{OSK}-transfected HEK293 cells. HEK293 cells were transfected with an APP_{WT} or APP_{OSK} construct and loaded with cholesterol. **A:** Cellular cholesterol levels increased significantly immediately after cholesterol loading (solid columns) compared with unloaded cells (open columns). After a 6-hr incubation for cholesterol efflux (shaded columns), APP_{WT}-transfected cells exhibited lower levels of cellular cholesterol than mock-transfected cells, whereas APP_{OSK}-transfected cells exhibited levels of cellular cholesterol that were similar to those of mock-transfected cells. Results are presented as mean ± SEM (n = 3–4). **B:** The concentrations of secreted Aβ were determined by ELISA. Both $Aβ_{40}$ and $Aβ_{42}$ in cultured media were lower in APP_{OSK}-transfected cells than in APP_{WT}-transfected cells. ND, not detected. **C:** Intracellular Aβ was extracted, and its levels were measured. APP_{OSK}-transfected cells exhibited significantly higher levels of intracellular $Aβ_{40}$ and $Aβ_{42}$ than APP_{WT}-transfected cells. Results are presented as mean ± SEM (n = 4).

bodies are larger than those of HEK293 and Neuro-2a cells, making this cell line more suitable for examining the subcellular localization of cholesterol and Aβ. APP expression (C40-positive) was confirmed in both APP_{WT}- and APP_{OSK}-transfected cells but apparent intracellular Aβ accumulation (82E1-positive) was observed only in APP_{OSK}-expressing cells (Fig. 3A). The cells were loaded with cholesterol for 30 min. All of the mock-, APP_{WT}-, and APP_{OSK}-expressing cells exhibited increased filipin staining in the plasma membrane immediately after cholesterol loading (Fig. 3B). After a 6-hr incubation with cholesterol-free medium, filipin-positive materials in these cells were largely sequestered within intracellular compartments, indicating that cholesterol was internalized into the cells (Fig. 3C). Notably, APP_{WT}-expressing cells exhibited only weak filipin staining after the 6-hr incubation, suggesting that internalized cholesterol was efficiently excreted from the cells during the incubation. Intracellular Aβ in APP_{OSK}-expressing cells remained to accumulate even after a 6-hr incubation. These observations are consistent with the biochemical results showing that the Osaka mutation has a defect in cholesterol efflux and Aβ secretion (Fig. 1). In APP_{OSK}-expressing cells, 59.0% ± 3.4% of cellular cholesterol was found to colocalize with Aβ (n = 26). Almost no change of APP localization was observed during cholesterol loading and subsequent incubation in both APP_{WT}- and APP_{OSK}-expressing cells, implying that APP trafficking is not involved in intracellular cholesterol transport and efflux.

Subcellular Localization of Aβ and Cholesterol in APP_{OSK}-Expressing Cells

It is known that, after internalization, cholesterol is transported from the endosomes to the ER and Golgi apparatus and then to the plasma membrane to be